

Multiscale single-cell analysis reveals unique phenotypes of raphe 5-HT neurons projecting to the forebrain

Sebastian Pablo Fernandez^{1,2,3} · Bruno Cauli^{2,4,5} · Carolina Cabezas^{1,2,3} · Aude Muzerelle^{1,2,3} · Jean-Christophe Poncer^{1,2,3} · Patricia Gaspar^{1,2,3}

Received: 7 July 2015 / Accepted: 2 November 2015 / Published online: 25 November 2015
© Springer-Verlag Berlin Heidelberg 2015

Abstract Serotonergic neurons of the raphe nuclei exhibit anatomical, neurochemical and electrophysiological heterogeneity that likely underpins their specific role in multiple behaviors. However, the precise organization of serotonin (5-HT) neurons to orchestrate 5-HT release patterns throughout the brain is not well understood. We compared the electrophysiological and neurochemical properties of dorsal and median raphe 5-HT neurons projecting to the medial prefrontal cortex (mPFC), amygdala (BLA) and dorsal hippocampus (dHP), combining retrograde tract tracing with brain slice electrophysiology and single-cell RT-PCR in Pet1-EGFP mice. Our results show that 5-HT neurons projecting to the dHP and the mPFC and the BLA form largely non-overlapping populations and that BLA-projecting neurons have characteristic excitability and membrane properties. In addition, using an unbiased clustering method that correlates anatomical, molecular and electrophysiological phenotypes, we find

that 5-HT neurons with projections to the mPFC and the dHP segregate from those projecting to the BLA. Single-cell gene profiling showed a restricted expression of the peptide galanin in the population of 5-HT neurons projecting to the mPFC. Finally, cluster analysis allowed identifying an atypical subtype of 5-HT neuron with low excitability, long firing delays and preferential expression of the vesicular glutamate transporter type 3. Overall, these findings allow to define correlated anatomical and physiological identities of serotonin raphe neurons that help understanding how discrete raphe cells subpopulations account for the heterogeneous activities of the midbrain serotonergic system.

Keywords Serotonin · Raphe · Galanin · Amygdala · Hippocampus · Prefrontal cortex · Single-cell PCR · Patch-clamp

Electronic supplementary material The online version of this article (doi:10.1007/s00429-015-1142-4) contains supplementary material, which is available to authorized users.

✉ Sebastian Pablo Fernandez
sebastian.fernandez@ipmc.cnrs.fr

✉ Patricia Gaspar
patricia.gaspar@inserm.fr

- ¹ Institut du Fer à Moulin, INSERM U839, 17 rue du Fer à Moulin, 75005 Paris, France
- ² Université Pierre et Marie Curie, Paris, France
- ³ Institut du Fer à Moulin, Paris, France
- ⁴ CNRS, UMR 8246, Neuroscience Paris Seine, 75005 Paris, France
- ⁵ Inserm UMR-S 1130, Neuroscience Paris Seine, 75005 Paris, France

Introduction

Serotonin (5-HT) has been implicated in a wide range of neurobiological functions, from neurovegetative to higher brain functions, including anxiety-related behaviors (Fernandez and Gaspar 2012), learning and memory (Buhot et al. 2000) and decision-making (Miyazaki et al. 2012). Whether one or several different 5-HT subsystems underlie this wide array of functions remains a matter of debate (Hensler 2006; Graeff and Zangrossi 2010; Andrade and Haj-Dahmane 2013). Because of their remarkable diffuse connectivity, it has generally been assumed that an individual 5-HT neuron of the raphe is capable of influencing multiple brain areas via volumetric transmission, and hence to simultaneously impact numerous functions (Bunin and Wightman 1999; Waselus et al. 2011).

Challenging the notion of a diffuse serotonergic system, however, there is a substantial body of evidence indicating a heterogeneity of the 5-HT raphe neurons (Calizo et al. 2011; Hale and Lowry 2011; Gaspar and Lillesaar 2012; Brust et al. 2014). Anatomically, a broad topographic organization of raphe projections has been shown, with the demonstration of a complementary innervation to the forebrain from the dorsal (DR) and median raphe (MR) (Jacobs et al. 1978; Vertes and Crane 1997; Vertes et al. 1999; Bang et al. 2012; Muzerelle et al. 2014). Electrophysiologically, raphe 5-HT neurons have a specific signature, characterized by low frequency and highly regular discharge. However, differences in excitability and membrane properties were also noted between cells in different raphe subnuclei (Trulsson and Frederickson 1987; Beck et al. 2004a; Crawford et al. 2010). In vivo recordings further showed the existence of fast, slow and bursting firing 5-HT neurons (Kocsis et al. 2006; Hajós et al. 2007) and a diversity of responses of DR neurons to salient stimuli (Ranade and Mainen 2009; Schweimer and Ungless 2010). Neurochemically, all 5-HT raphe neurons share a common identity (Deneris and Wyler 2012), but they also differ in their co-neurotransmission properties (Gaspar and Lillesaar 2012). Subsets of DR 5-HT neurons endow glutamate co-neurotransmission (Johnson and Yee 1995; Amilhon et al. 2010; Liu et al. 2014) and some neurons contain peptides such as galanin (Melander et al. 1986), substance P (Chan-Palay et al. 1978), or corticotropin-releasing hormone (Commons et al. 2003). Overall, these studies suggest that there may be distinct raphe circuits underlying specific roles of 5-HT in behavioral control.

A desirable goal then is to obtain a general model combining defined anatomical, electrophysiological, and neurochemical properties and to identify functionally relevant 5-HT cell types. Such scheme is essential to understand the cellular basis for the temporal and regional selectivity of serotonergic signalling in the brain, as it has been demonstrated for other monoamines such as dopamine neurons in the VTA (Lammel et al. 2008; Margolis et al. 2008), and, more recently, noradrenergic cell types in the locus coeruleus (Chandler et al. 2014). Here, we focused on the 5-HT raphe neurons that project to the medial prefrontal cortex (mPFC), the basolateral amygdala and (BLA) the dorsal hippocampus (dHP). Combining retrograde tracing with patch-clamp recordings and single-cell RT-PCR, we obtained multiple electrophysiological and neurochemical features of single raphe 5-HT neurons. We show that serotonergic neurons projecting to the BLA form a non-overlapping subpopulation with clear differences in excitability and membrane properties compared to neurons that project to the mPFC and dHP. We extended the analysis to a broad neuronal population of DR and MR neurons, and provide the first unbiased classification of

5-HT raphe neurons based on multiple criteria. The statistical robustness of this model was confirmed using multiple discriminant analysis. Furthermore, our results indicate that markers of co-neurotransmission such as galanin and vesicular glutamate transporter 3 (Vg3) relate to specific firing patterns of raphe neurons, and forebrain projections.

Materials and methods

Animals

All experiments were performed in compliance with the standard ethical guidelines (European Community Guidelines and French Agriculture and Forestry Ministry Guidelines for Handling Animals—decree 87849).

A Pet1-EGFP mouse line was used to visualize 5-HT neurons, on brain slices. Mice that carry a transgene expressing Cre recombinase specifically in serotonergic neurons, ePet1-Cre (Scott et al. 2005), were crossed with a reporter line to monitor Cre expression. The Rosa-26 reporter mouse line expressing enhanced green fluorescent protein (eGFP) (Sousa et al. 2009), was used for this purpose, as its usefulness for slice electrophysiology was previously demonstrated. C57-B16-J mice (CER-Janvier, France) were used in addition for histology. The total number of mice used was as follows: 16 mice for the anatomical study involving paired injections of retrograde tracer, 10 mice for electrophysiological recordings of retrograde labelled 5-HT neurons, and 24 mice for recording of 5-HT neurons without known projection target.

Retrograde labelling and histology

3–4 weeks C57-B16-J male mice were anesthetized with ketamine (50 mg/kg) and xylazine (2 mg/kg) and fixed in a stereotaxic apparatus. Stereotaxically guided injections were made through holes in the dorsal surface of the cranium. Glass capillary tubes (PCR micropipette, Drummond Scientific Company) were pulled (HEKA pipette puller PIP5) and tips broken to 40 μ m diameter. Capillaries were filled with green or red fluorescent RetroBeads (Lumafuor, USA) fixed to an adapter designed to be mounted on the oil hydraulic micromanipulator MO-10 (Narishige, Japan). Positive pressure was applied to the capillary during 5 min to inject a total volume of 200 nl per site. Paired unilateral injections were directed to the dorsal hippocampus (−1.7 mm Bregma, 1.0 mm mediolateral and 2.0 mm dorsoventral) and the infralimbic prefrontal cortex (+1.6 mm Bregma, 0.3 mm mediolateral and 3.1 mm dorsoventral), or to the infralimbic prefrontal cortex and the basolateral amygdala (−1.7 mm Bregma, 3.2 mm

mediolateral and 4.6 mm dorsoventral). In addition, four cases received paired injections of red and green Retrobeads into the prefrontal cortex. The coordinates were obtained from the atlas “The Mouse Brain In Stereotaxic Coordinates” (second edition, G. Paxinos, K. Franklin, Academic Press 2001), and checked in pilot experiments. Micropipettes were left in place 5 min before removal to minimize leakage.

After a 4–7 day survival period, the animals were anesthetized with pentobarbital (0.5 mg/g) and fixed by intracardiac perfusion of 4 % paraformaldehyde in 0.1 M phosphate-buffered saline (pH 7.4). Brains were post-fixed overnight in the same fixative solution and cryoprotected during 2 days in 30 % sucrose containing sodium azide (0.01 %; Sigma-Aldrich Co., MO, USA). Serial coronal sections (50 μ m thick) were obtained on a cryo-microtome (Microm Microtech, France), and collected as series of 6 in the forebrain and series of 3 in the hindbrain. The location of the paired injection sites was first checked on the forebrain series, and cases with misplaced injections or showing leakage of dyes in the ventricle were discarded from the study. Hindbrain serial sections including the raphe were either mounted directly in Mowiol 10 % (Calbiochem, Germany) and Dabco 2.5 % (Sigma-Aldrich Co., MO, USA), or after TPH immunostaining. A standard immunostaining protocol (see Kiyasova et al. 2011) was used to reveal TPH2 (goat anti-TPH2, Millipore, 1/2000) using far red fluorochrome (donkey anti-goat Alexa 678). Immuno-cytochemical characterization of the Pet1-GFP mice was done on brain sections of 1–2 months old mice. The following primary antibodies were used: Chicken anti-GFP (Aves Labs, 1/1000), rabbit anti -5-HT (Cambiochem, 1/5000); rabbit anti-galanin (Peninsula lab, 1/2500) and the following secondary antibodies: Alexa 488-Donkey anti-chicken, Cy3-Donkey anti rabbit (Jackson Immuno Research, Europe Ltd).

Cell counts

Counts of single and double retrogradely labelled neurons in the raphe were done on one complete series of sections (1/3) through the brainstem (Paxinos levels –4 to –5.2 from Bregma; typically 8 sections in one series). The DR and MR were scanned with a Leica DM6000 microscope (40 \times final magnification) and the number of retrogradely labeled neurons containing, either green, red, or both red and green beads was counted in each section to compute the total number of retrogradely labeled neurons in the raphe from each target, and cells showing co-labelling from both targets.

In another series of sections immunostained with TPH2 we estimated the percentage of retrogradely labeled neurons that are serotonergic using confocal microscopy.

Selected sections containing the largest number of retrogradely labelled neurons were analyzed with a TCS SP5 II (Leica), using 3 different laser beams (488, 514, and 633) to sequentially detect the green, red and far red fluorescence. Confocal images (1 μ m thick 40 \times objective) were acquired at 1024 \times 1024 pixel resolution, with pinhole set to one Airy unit. In each case 3 different images were collected in both the DR and MR to estimate the number of retrogradely labelled neurons that were or not co-localized with TPH2-immunocytochemistry.

Electrophysiological recordings and scRT-PCR amplification

Electrophysiological recordings and molecular characterization of 5-HT neurons was conducted in acute brain slices from male Pet1-EGFP mice aged 3–4 weeks old. One series of mice received injections in the mPFC, dHP or BLA of red RetroBeads (Lumafuor, USA) 5–6 days before preparation of slices. The methodology and coordinates for stereotaxic injections were as above, except that only a single brain structure was injected bilaterally per animal. Another series of mice were naïve. In all cases, on the day of the recording, mice were decapitated and the brain was rapidly dissected out. Coronal slices (250 μ m) containing the DR and MR were prepared with a vibratome (Microm HM650 V, Thermo Scientific) and placed in aCSF containing (in mM): 11 glucose, 2.5 KCl, 26.2 NaHCO₃, 1 NaH₂PO₄, 124 NaCl, 2 CaCl₂, 2 MgCl₂ bubbled with a mixture of 95 % O₂/5 % CO₂. After a 1-h recovery period, individual slices were placed in an electrophysiology chamber continuously perfused with aCSF maintained at 31 °C. Neurons were visualized by combined epifluorescent and infrared/differential interference contrast visualization using an Olympus BX51WI upright microscope holding 5 \times and 40 \times objectives. Expression of green fluorescent protein was detected with a Endow GFP/EGFP Bandpass filter (Chroma Technology Corp, USA, #41017), and presence of red microspheres with a TRITC (Rhodamine)/DiI/Cy3 filter (Chroma Technology Corp, USA, #31002). Borosilicate glass pipettes (3–5 M Ω) were made in a HEKA PIP5 puller and filled with 8 μ l of autoclaved RT-PCR internal solution (in mM): 144 K-gluconate; 3 MgCl₂; 0.5 EGTA; 10 HEPES, pH 7.2 (285/295 mOsm). Single EGFP-positive neurons were approached with a pipette and whole-cell recordings were obtained using a Multiclamp 700B (Molecular Devices, Sunnyvale, CA, USA). Signals were collected and stored using a Digidata 1440A converter and pCLAMP 10.2 software (Molecular Devices, CA, USA). Current steps of 500 ms were injected starting at –40pA and increasing in 20pA steps to a maximum of +240pA. To avoid dialyzation of the cells and therefore decrease scRT-PCR success rate, recordings

always lasted less than 5 min. In order to describe the electrophysiological features of 5-HT neurons, a total of 23 electrophysiological parameters were determined for each cell from recordings made in current-clamp mode (Karagiannis et al. 2009). Passive membrane characteristics included: resting membrane potential defined as the voltage at which $I = 0$; input resistance (R_m) and membrane time constant (τ_m) were measured on responses to a -20 -pA hyperpolarizing current pulse (Karagiannis et al. 2009). Membrane capacitance (C_m) was calculated according to the equation $C_m = \tau_m/R_m$. Rheobase was defined as the first current pulse to elicit an action potential, and the first spike latency at rheobase was also measured. Action potential amplitude was measured from threshold to the positive peak, and the duration was measured at half amplitude. The shape of the first spike's after hyperpolarization potential was also monitored, including amplitude at the peak, and the decay and recovery times measured at half amplitude. In the last current pulse the amplitude and latency of the first spike were measured. First spike amplitude was compared to the amplitude of the second and last spike in the same train to determine spike amplitude reduction. Maximal frequency was also calculated in the last pulse trace. The instantaneous discharge frequency was determined for all current pulses and plotted as a function of time. To account for the early and late frequency adaptation phenomena, instantaneous frequency was fitted to a single exponential with a sloping base according to $F_{\text{saturation}} = A_{\text{sat}} e^{-t/\tau_{\text{sat}}} + t m_{\text{sat}} + F_{\text{max}}$, where A_{sat} is the amplitude of the early adaptation, τ_{sat} is the time constant of early adaptation, m_{sat} is the slope to late adaptation and F_{max} is the maximal steady state frequency (Karagiannis et al. 2009).

The methodology involved in harvesting of cytoplasmic content and subsequent single-cell PCR amplification has been described previously (Cauli et al. 2000). In brief, after electrophysiological recording, the cytoplasmic content of the cell was harvested by applying gentle negative pressure to the pipette. Cell content was expelled into a tube where a reverse transcription reaction was performed in a final volume of 10 μl . cDNA sequences were thereafter amplified by conducting a multiplex nested PCR, designed to simultaneously detect a series of molecular markers. The complete list of genes investigated is indicated in Table 1. Initially, all genes were simultaneously amplified in a single tube using 10 μl of cDNA, 200 nM of each primer and 2.5 U of Taq polymerase in a final volume of 100 μl . PCR reaction was carried out using 6 min hot start at 94 $^{\circ}\text{C}$, followed by a 21-cycles program (94 $^{\circ}\text{C}$ for 30 s, 60 $^{\circ}\text{C}$ for 30 s and 72 $^{\circ}\text{C}$ for 30 s). Subsequently, 2 μl of the amplified cDNA was used as the template for the second amplification step. Here, each gene was individually amplified in a separate tube submitted to a 35-cycles

PCR program using the same conditions as mentioned above, in a final volume of 100 μl . The products of the second PCR were analyzed by electrophoresis in 2.5 % agarose gels using SYBR safe gel stain (Invitrogen, Oregon, USA). When possible, primer pairs were designed to amplify cDNA regions spanning at least one intron, except for intron-less genes such as CB1 and 5-HT1A receptors. In order to control that PCR amplification was not due to nuclear DNA contamination an additional primer pair was included to amplify a somatostatin intron sequence (Hill et al. 2007). The size of the PCR-generated fragments was as predicted by the mRNA sequences. The scRT-PCR procedure was tested by synthesizing cRNA for the Tph2 gene from a plasmid construct to carry out the protocol. This allowed establishing a detection limit of 0.9415 pg of cRNA. In order to control that scRT-PCR amplifications corresponded to specific material coming from the patched cell and not from contamination, two forms of negative controls were carried out on a regular basis. First, a no template control where cell content was replaced by distilled water. Second, a tissue debris control where a pipette filled with RT-PCR internal solution was driven slightly into the brain slice and negative pressure was applied. In both cases, the samples were used to run parallel scRT-PCRs; in none of these experiments amplification of the targeted genes was observed.

Data analysis

In order to explore whether the variance observed in electrophysiological parameters could be reduce to a few composite constructs, and therefore identify discriminant parameters in different projecting neurons, retrogradely labeled neurons were first subjected to a principal component analysis using STATISTICA software (StatSoft, Tulsa, OK, USA). Data were normalized and converted to Z-scores, and the analysis was performed on the correlation matrix using the NIPALS algorithm with a maximum of 50 iterations and convergence factor of 0.0001. Obtained components with Eigenvalues >1 were considered in subsequent analysis (Kaiser 1960).

To achieve an unbiased classification of 5-HT neurons, unsupervised clustering was performed using Ward's method (Ward 1963). First, anatomical and molecular nominal variables were coded to numerical variables. For anatomical localization the dorso-ventral axis was assigned values of: dorsal = 0 and ventral = 1, and for the medial-lateral axis: medial = 0 and lateral = 1. Molecular data was coded as 0 when the PCR product was absent in the agarose gel and 1 when present. Second, the anatomical, molecular and electrophysiological parameters were standardized by centering and reducing all of the obtained values. Finally, cluster

Table 1 List of genes amplified by nested single-cell PCR, and the internal and external primer pairs used

Acronym	Gene name	GenBank accession number	External primer pair	Product size (bp)	Internal primer pair	Product size (bp)
TPH2	Tryptophan hydroxylase 2 (Tph2)		CCCGGAACCAGATACATGCC	262	TGGGATCCCAAGTTTGCTC	160
	NM_173391.2		TTTACACACAGCCTTGTCCGG		TAACCCGTCCCATACGCC	
VG3	Glutamate vesicular transporter, member 8 (Slc17a8)		ACGGCTGTGTTCATGGGTGTG	265	CCTGCCATGGGATGTGGAGT	149
	NM_182959.2		TAAGCCTGCAGCAGCCAAA		AAAGACAGAGGCCACAGCCAA	
TAC1	Tachykinin 1		TGAAAAATCCCTCGTGGCCGT	175	TGCAGAGGAAAATCGATGCCA	100
	NM_009311.2		GGTCTTCGGGCGGATTCTCTG		AAGATGCTCAAAGGGCTCCG	
GAL	Galanin		GGCTGGCTCCTGTGGTTGT	288	CACTCTGGACTTGGGATGC	162
	NM_010253.3		AGGCAGGGGCACATCAACAC		CTCCTTCTCCACCTCCAGTT	
NOS	Nitric oxide synthase 1, neuronal		TGCCCATGGTTCTGGTCTT	274	ACCCTGCAGGCCAAGAACA	131
	NM_008712.2		TTATGCGCTGGATGGCTTIG		AGGGCGGTACACAGACTC	
CCK	Cholecystokinin		TGTCTGTGCGTGGTGTGGC	554	ATACATCCAGCAGGTCCGCAA	219
	NM_012829.1		GCATAGCAACATTAGGTCTGGGAG		GGTCTGTGCGTGGTGTGTT	
Adre α 1b	Adrenergic receptor, alpha 1b		GGCGGGAGTCATGAAGGAAA	328	AGCAGTACCAAGGCCAAGGG	171
	NM_007416.3		GATGATGGGGTTGAGGCAGC		GGTGGAGAACAAGGGAGCCAA	
Hista R1	Histamine receptor H1		TCCTTCTCCGGACCACAGA	307	TGTGTCCGGTTGCACCTGA	130
	NM_008285.3		AGCCAGCCAAATGGTGAAC		GCAGCTGTTGCAGAAAGCCAA	
Oxy R	Oxytocin receptor		TGCAGATGTGGAGCGTCTGG	261	GTCAATGGCCCCAAAAGAAC	161
	NM_001081147.1		TCTGACTCGAGCTGCGACGA		CTGCCCTTACAGTACCGAGC	
Nic α 7	Cholinergic nicotinic receptor alpha 7		CTCATGGGAATCCCTGGCAA	316	CTCATGGGAATCCCTGGCAA	158
	NM_007390.3		TGATCATGGTGTCTGGCGAAG		AGCAAAGCCAGGGCTGAAAT	
Orex R1	Hypocretin (orexin) receptor 1		CGATACCTGTGGCGGATTA	298	GCAATACCCCTGGTCTGCCTG	177
	NM_198959.1		CTGACACCGACACAGCCTGG		TGACCTTGCACAAAAGCCTGG	
Orex R2	Hypocretin (orexin) receptor 2		TCGGGAACGTCTGGTCTGT	310	CTGCCCTTCCAGTACCCTCG	135
	NM_198962.3		ATGCTGTTTCGAGCCCGTTT		TCCAAAGGCAATGCAGCTCAA	
GABAA α 1	GABAA α 1 subunit		CAAGAGGGGTATGCGTGGG	282	GGATGGCAAAAAGCTGGTTC	198
	NM_010250		CCAAATAGCAGCCGAAAAGGC		TTGGGTTCTGGTGGTTTTGTCT	
GABAA α 2	GABAA α 2 subunit		CTCCCGATGGCTCCAGGTTA	227	GGCCAGTCAATTTGGGAAGGA	161
	NM_008066.3		CACAGTTCTTGTGGCACCCG		TTCAGCCAGAATGACACTTGGGA	
GABAA α 3	GABAA α 3 subunit		TCGACCTGGACTTGGAGATGC	334	CCAGTTTGGCCCTGTGTCA	112
	NM_008067.3		CATGGGCATTCAGCGTGTGA		GGAAAGATCTTCATTTGGTCCATCA	
GABAB	GABAB 1a subunit		GGCATCAGGTACCGTGGCTT	286	GACTCGGACCAGGTGAAGG	133
	NM_019439.3		AGTCGGGTTCACATCGGAAA		CATATCCGTCCAGGACCGT	
5-HT1A	5-hydroxytryptamine receptor 1A		CAGCCAGGTAGTGGGGACTG	260	CGGTGAGACAGGGGTAGGAC	118
	NM_008308.4		GTCTTCTCTCACGGGCCAA		GCGGGGACATAGGAGGTAGC	

analyses were run on STATISTICA software (StatSoft, Tulsa, OK, USA). Parameters included in the cluster analysis were as follows: anatomical localization dorso-ventral (1), medio-lateral (2), resting potential (3), membrane resistance (4), time constant (5), capacitance (6), rheobase (7), first spike latency (8), spike threshold (9), action potential amplitude (10) and duration (11), AHP amplitude (12) and duration (13), last train spike amplitude reduction (14), maximal discharge frequency (15), amplitude of early frequency adaptation (16), time constant of early adaptation (17), maximal steady-state frequency (18), slope of late adaptation (19), vesicular glutamate transporter 3 (20), galanin (21), cholecystokinin (22), tachykinin (23) and nitric oxide synthase (24). Briefly, the cluster analysis consists in first grouping the closest individuals (each of them being represented by a point in a multidimensional space) by using the matrix of their Euclidean distances. Then, at each stage, the number of groups is reduced by one (or more) by merging two groups (or individuals) whose combination gives the least possible increase in the within-group sum-of-squares deviation. This method is usually implemented through updating a stored matrix of Euclidean distances between cluster centroids. Average within-cluster distance shown in Fig. 5a represents the Euclidean distance between the centroids of the merged clusters. The final number of clusters was suggested by the Thorndike procedure where the average within-cluster distance is plotted at each stage of the amalgamation schedule, resulting in a decrease in the average within-cluster distance as the number of clusters increases (Thorndike 1953). The final number of classes (or cell types) is determined at the stage where the maximal decrease is reached in this plot.

To evaluate the significance in the variability observed in electrophysiological properties, raw unstandardized data coming from current-clamp recordings were compared using parametric one- or two-way ANOVA tests, followed by Bonferroni's post hoc comparisons (STATISTICA). Comparison of the occurrence of a given molecular marker between clusters of 5-HT neurons was done using the following equation:

$$|\varepsilon| = \frac{|pa - pb|}{\sqrt{\frac{pq}{n_a} + \frac{pq}{n_b}}}$$

where p_a and p_b are the occurrence, and n_a and n_b the number of individuals in populations a and b. The variable p denotes the occurrence in the overall population, and $q = 1 - p$. This quantity ε was tested against a normal distribution to determine statistical significance (Toutenburg 1971)

Fig. 1 Dual retrograde labelling of neurons in the mouse raphe nucleus. **a–c** Representative case of a dual injection to the dorsal hippocampus (dHP) and the medial prefrontal cortex (mPFC) is shown. **a** Green retrobeads were injected in the mPFC, and red beads in the dHP. **b** Schematic representation showing the position of the retrogradely labelled neurons at 3 rostrocaudal levels of the raphe nuclei. *Green* (mPFC), *red* (dHP) and *yellow* (PFC + dHP) circles indicate individual retrogradely labelled neurons. **c** Confocal image in the MR showing the 2 colour beads and Tph2 immunocytochemistry. *Arrowheads* point to neurons projecting to the dHP (*red*) and *arrows* to the mPFC (*green*). *Scale bar* 50 μ m. **d** *Bar graph* shows the mean \pm SEM of the number of raphe cells back-labelled from the mPFC (*green*), the dHP (*red*) or both (*yellow*). Counts are the sum of labelled neurons from 5 sections spaced by 200 μ m through the raphe for each case ($n = 4$ mice). **e** Representative case of dual injection in the mPFC and the basolateral amygdala (BLA). **f** Topography of retrogradely labelled neurons in the raphe at 3 rostro-caudal levels through the raphe. **g** Confocal image in the DRM showing the 2 colour beads and Tph2 immunocytochemistry. *Arrowheads* point to neurons projecting to the BLA (*red*) and *arrows* to the mPFC (*green*). *Scale bar* 50 μ m. **h** *Bar graph* shows the mean \pm SEM of the number of raphe cells back-labelled from the mPFC (*green*), the BLA (*red*) or both (*yellow*). Counts are the sum of labelled neurons from 5 sections spaced by 200 μ m through the raphe for each case ($n = 4$ mice)

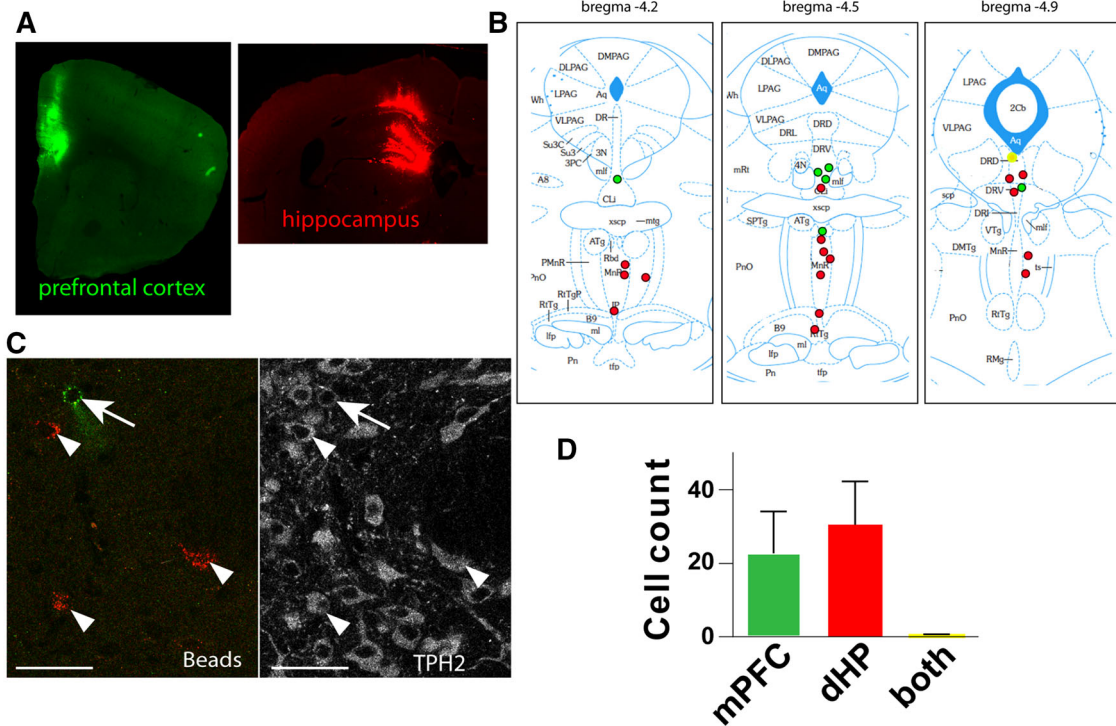
Results

5-HT neurons projecting to the mPFC, the BLA and the dHP are segregated

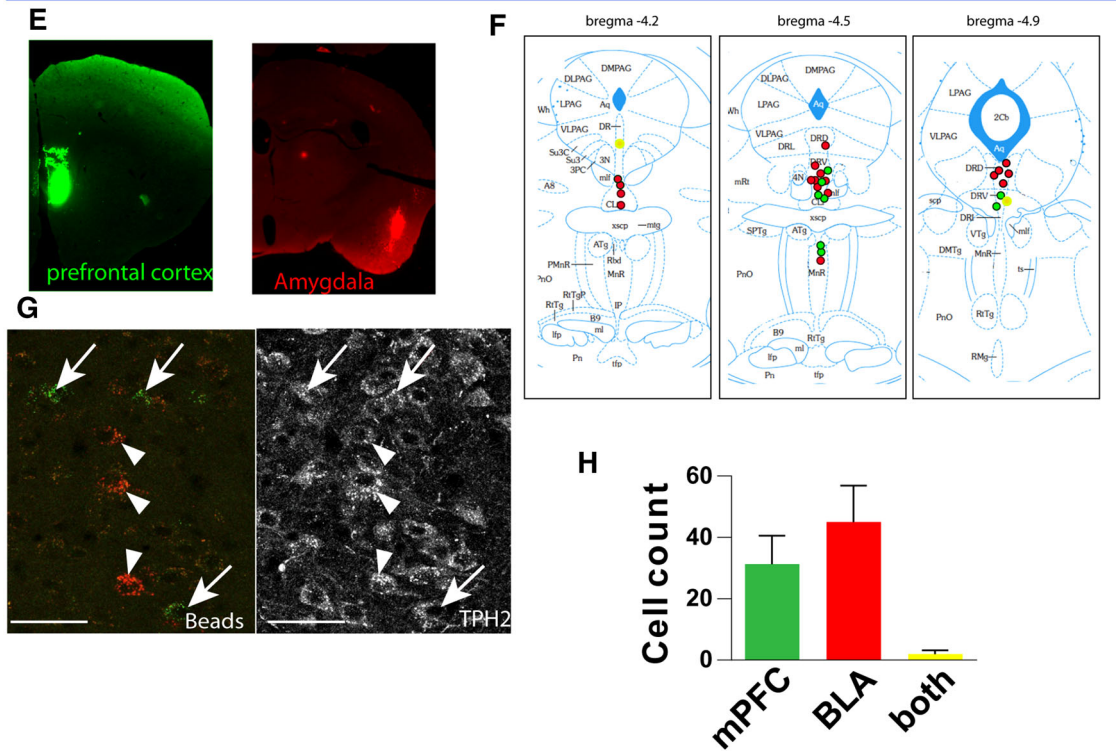
A substantial number of anterograde and retrograde anatomical studies have indicated the existence of a broad topographic organization of the DR and MR projections (Jacobs et al. 1978; Vertes and Crane 1997; Vertes et al. 1999; Bang et al. 2012; Muzerelle et al. 2014). These studies showed that most of the projections to the amygdala originate from the dorsal raphe medialis (DRM), a majority of the hippocampal 5-HT innervation is derived from the MR, while the mPFC receives inputs from both the DRM and MR. However, analysis of individual raphe neurons showed that single raphe neurons have highly branched axons that can reach several targets such as the mPFC and amygdala (Gagnon and Parent 2014). To evaluate the extent to which DR and MR neurons collateralize to the BLA, mPFC, and dHP we used red and green retrobeads in different combinations. Beads have the advantage of a restricted diffusion radius compared to other retrograde tracers allowing precise analysis of dual labelling. However, it should be noted that given this limited diffusion, beads are taken up only by axon terminals that lie close to the injection site, and likely requires that a sufficient number of terminal uptake the tracer.

In a first set of control experiments, we paired the injections of both green and red fluorescent beads in the mPFC. This showed a 100 % of co-labelled neurons in many nuclei projecting to the mPFC, including the medial

Case mPFC-dHP-12



Case mPFC-BLA-13



thalamus, the DR and the MR (Fig. S1), validating the fact that both tracers have the same diffusion and transport rate. To evaluate the potential collateralization to the dHP and the mPFC, dual injections of red and green microspheres

were performed (Fig. S1, $n = 4$). Hippocampal projecting neurons were mainly localized in the MR, with rare neurons in the DRM, except in the caudal-most part, that corresponds to the B6 cell group where hippocampal back-

labelling was observed (Fig. 1b). The mPFC-projecting neurons were localized in both the DRM and MR with predominance in the DRM (Fig. 1f). Despite moderate topographic overlap, co-localization of the two tracers was rarely observed in the dual injections: among the 122 hippocampal projecting neurons and the 91 mPFC-projecting neurons identified only 2 were dually labelled (Fig. 1d). Collateralization of raphe neurons to the mPFC and the BLA was analyzed using the same dual injection approach (green retrobeads in the mPFC and red retrobeads in the BLA, Fig. 1e). In these cases ($n = 4$), the BLA and mPFC-projecting raphe neurons were intermingled with no obvious topography in the DR (Fig. 1f). Quantification on serial sections revealed that among the 125 mPFC-projecting neurons and the 180 amygdala projecting neurons identified only 8 were dually labelled (Fig. 1h). We also performed dual injections in the BLA and the dHP, and, as expected, we did not find any co-labelling of neurons (data not shown); this is in agreement with the data presented here and previous reports showing that raphe neurons projecting to the BLA are located in the DRM, and those projecting to the dHP in the MR (see above). Overall, these results showed that despite some degree of collateralization, different raphe neurons target the 3 forebrain areas analyzed.

Tph2 immunostaining was used to estimate the proportion of back-labelled neurons that are serotonergic (Fig. 1i). A majority of raphe projection to the mPFC and amygdala were co-labelled with Tph2 (mPFC 80 %, $n = 56$ neurons; BLA 74 %, $n = 118$ neurons). While only about half of the raphe neurons projecting to the dHP ($n = 40$ neurons) were serotonergic, confirming previous observations (Köhler and Steinbusch 1982; Kiyasova et al. 2011). This indicated the requirement of a genetic labelling of 5-HT identity to analyze further the electrophysiological and neurochemical properties of the 5-HT raphe neurons targeting these different structures. We, therefore, used a reporter mouse line (Pet1cre-EGFP) in which over 95 % the dorsal and medial raphe neurons co-express the bright fluorescent reporter eGFP (Fig. S2) (Kiyasova et al. 2013).

5-HT cell characteristics vary according to projection target

To study cellular and molecular characteristics in target-defined populations of 5-HT neurons, retrograde neuronal tracing was combined with patch-clamp recordings followed by scRT-PCR analyses. Red microspheres were injected in the BLA, the mPFC or the dHP of Pet1cre-EGFP mice and retrogradely labeled GFP-expressing 5-HT neurons were patched, recorded, and characterized by scRT-PCR (Fig. 2). Representative photomicrographs depicting the morphological identification of back-labeled

5-HT neurons during patch-clamp recordings are shown in Fig. 2a. A total of 58 5-HT neurons were characterized, including 19 neurons projecting to the BLA ($n = 3$ mice), 20 neurons to the mPFC ($n = 4$ mice) and 19 neurons to the dHP ($n = 3$ mice). The anatomical localization of the neuron recorded can be found in Table S1.

All recorded 5-HT neurons were spontaneously silent, in agreement with previous observations (Aghajanian and Vandermaelen 1982; Vandermaelen and Aghajanian 1983); therefore, characterization was achieved by injecting current steps of increasing intensity. Identified projection neurons differed in their excitability: BLA-projecting neurons showed lower excitability than mPFC- and dHP projecting 5-HT neurons (Fig. 2c–e). BLA-projecting 5-HT neurons fired significantly less action potentials than those projecting to the mPFC and dHP (Fig. 2c, d). The number of spikes vs current injection plots is shown in Fig. 2d; two-way ANOVA (target region vs input current) showed that the main effect of target region ($F = 3.514$, $p < 0.05$) and current injection ($F = 529.5$, $p < 0.001$), (as well as their interaction $F = 4.005$, $p < 0.001$) were significant. Post hoc Tukey's multiple comparisons test of the main effect showed that BLA-projecting neurons elicited significantly less spikes (Fig. 2c). Consistently, the maximal discharge frequency of BLA-projecting neurons was significantly lower than mPFC and dHP terminal 5-HT neurons (one-way ANOVA, $F = 5.690$, $p < 0.01$, Fig. 2d). In addition, BLA-projecting neurons showed a significantly longer first spike delay than mPFC and dHP terminal 5-HT neurons ($F = 5.691$, $p < 0.01$, Fig. 2e).

Because action potential and after hyperpolarization potential (AHP) amplitude and duration are commonly used as criteria for identifying putative 5-HT neurons (Ranade and Mainen 2009; Calizo et al. 2011), we investigated their characteristics in these cell subpopulations. BLA-projecting 5-HT neurons showed spikes of longer duration ($F = 7.278$, $p < 0.01$ BLA vs dHP, Fig. 3a) and greater amplitude ($F = 3.113$, $p < 0.01$ BLA vs mPFC, Fig. 3a). Also, the AHP of BLA-projecting 5-HT neurons showed significantly smaller amplitude ($F = 5.859$, $p < 0.01$ BLA vs mPFC, Fig. 3b), and longer decay time ($F = 12.58$, $p < 0.01$ BLA vs mPFC, Fig. 3b). Passive membrane properties also showed differences with 5-HT cells projecting to the BLA having higher input resistance (BLA = $1218 \pm 154 \text{ M}\Omega$, dHP = $1050 \pm 84 \text{ M}\Omega$ and mPFC = $1118 \pm 154 \text{ M}\Omega$, $F = 2.106$, $p < 0.05$, one-way ANOVA) and larger time constant (BLA = $81.84 \pm 7.44 \text{ ms}$, dHP = $61.56 \pm 8.36 \text{ ms}$ and mPFC = $58.82 \pm 7.32 \text{ ms}$, $F = 3.713$, $p < 0.01$, one-way ANOVA) compared to those projecting to the dHP and the mPFC. Thus, these electrophysiological parameters vary among 5-HT raphe neurons and may be useful to distinguish specific cell subpopulations. This also indicates that one has to be

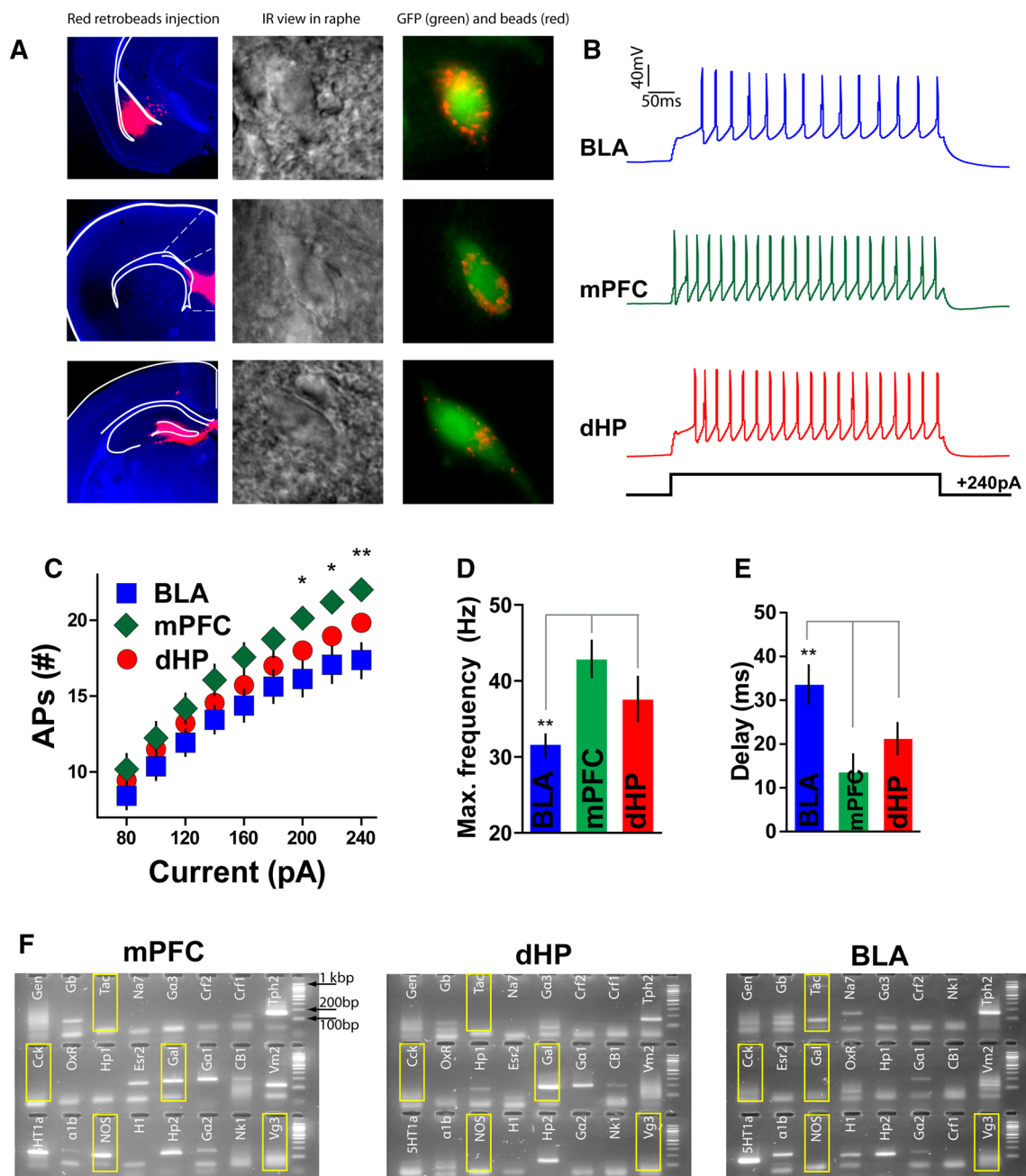
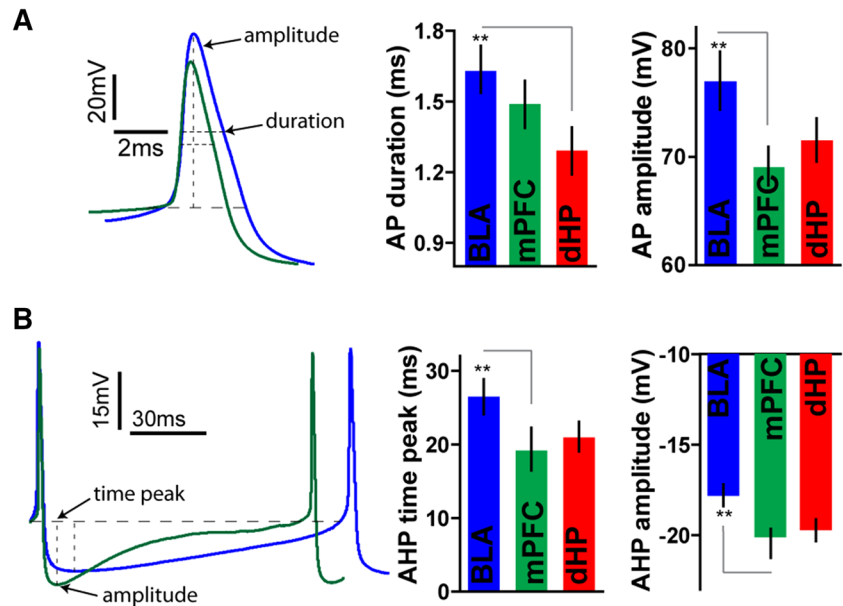


Fig. 2 Raphe 5-HT neurons projecting to the BLA have different properties than those projecting to the dHP and the mPFC. **a** Coronal sections in blue counter-staining (DAPI) showing representative locations of red microspheres injection sites in the BLA, the mPFC, and the dHP. Identification of back-labeled (red) GFP-expressing 5-HT neuron (green), and corresponding infrared image as seen in the recording setup. **b** Voltage responses of distinct target-specific 5-HT neurons to a +240pA current injection. **c** Number of action potentials vs current injection plots. Two-way ANOVA (target region vs input current) showed that the main effect of target region ($F = 3.514$, $p < 0.05$) and current injection ($F = 529.5$, $p < 0.001$), (as well as their interaction $F = 4.005$, $p < 0.001$) were significant. Post hoc Tukey's multiple comparisons test of the main effect indicates that BLA-projecting neurons discharge significantly less spikes. **d** Maximal discharge frequency of BLA-projecting neurons was significantly lower than mPFC and dHP projecting 5-HT neurons (one-way

ANOVA, $p < 0.01$). **e** First spike delay was also significantly higher in BLA-projecting neurons ($p < 0.01$). Data are expressed as mean \pm SEM, $n = 19$ (dHP), 19 (BLA) and 20 (mPFC). **f** Representative agarose gels showing the differential mRNA expression in target-specific Tph2-expressing 5-HT neurons as determined by scRT-PCR. Yellow boxes depict the presence/absence of genes related with co-transmission. Tph2 tryptophan hydroxylase 2, NOS nitric oxide synthase, Gal galanin, Vg3 vesicular glutamate transporter 3, TAC tachykinin, CCK cholecystokinin, $\alpha 1b$ adrenergic $\alpha 1b$ receptor subunit, HP1 and HP2 hypocretin receptors, HI histamine 1 receptor, Esr 2 estrogen receptor 2, OXR oxytocin receptor, Na7 nicotinic $\alpha 7$ receptor, CRF1 and 2 corticotrophin-releasing factor receptor 1 and 2, NK1 neurokinin 1 receptor, Gx1, 2 and 3 GABAA receptor α subunits, Gb GABAB receptor 1a subunit, Cb1 cannabinoid receptor, Gen, intron genomic control, 5-HT1a 5-HT receptor subtype 1A

Fig. 3 Differences in action potential and AHP shape in target-specific 5-HT neurons. **a** Representative action potential traces of a BLA- and a mPFC-projecting 5-HT neuron. BLA-target cells have spikes of longer duration ($p < 0.01$) and greater amplitude ($p < 0.01$). **b** After hyperpolarization potential (AHP) traces; BLA-projecting 5-HT neurons showed significantly smaller amplitude ($p < 0.01$), and longer decay time ($p < 0.01$). Data are expressed as mean \pm SEM, $n = 19$ (dHP), 19 (BLA) and 20 (mPFC)



cautious when using only electrophysiological criteria to identify 5-HT neurons.

After the recordings, the molecular phenotype of retrogradely labeled 5-HT neurons was profiled by scRT-PCR (Fig. 2f). The identity of the GFP-patched neurons was confirmed by amplification of the tryptophan hydroxylase (TPH2) gene. Because the number of genes that can be simultaneously assayed by scRT-PCR is limited, the choice of candidate genes was based on previous reports of differential expression among the MR and DR 5-HT neurons (see complete list in Table 1). Despite the differences in excitability patterns described above, we found little variation in the level of occurrence of common excitatory or inhibitory receptors among 5-HT neurons projecting to the mPFC, dHP and BLA, including adrenergic $\alpha 1$ receptor, hypocretin 1 and 2 receptors, histamine 1 receptor, oxytocin receptor, nicotinic $\alpha 7$ receptor, corticotrophin-releasing factor receptor 1, neurokinin 1 receptor, $\alpha 1$, 2 and 3 GABAA receptor, GABAB receptor 1a subunit and cannabinoid receptor (data not shown). We focused then on five genes that could pinpoint phenotypic co-transmission properties in 5-HT neurons, namely vesicular glutamate transporter 3 (Vg3), galanin, cholecystokinin (CCK), tachykinin, and nitric oxide synthase (NOS). Representative agarose gels pictures of scRT-PCR from individual cells are shown in Fig. 2f. The number of serotonergic neurons that express neuropeptide galanin was significantly higher in dHP (17 out of 19 cells) and mPFC (17 out of 20 cells) projecting neurons, compared to those projecting to the BLA (4 out of 19 cell, $\varepsilon = 2.63$, $p < 0.01$). Conversely, there was no significant difference in the number of cells expressing NOS (9/19 in dHP, 10/19 in BLA, 12/20 in mPFC, $\varepsilon = 0.51$, $p > 0.05$), Vg3 (4/19 in dHP 2/19 in

BLA, 3/20 in mPFC, $\varepsilon = 0.23$, $p > 0.05$) or tachykinin (3/19 in dHP, 4/19 in BLA, 3/20 in mPFC, $\varepsilon = 0.19$, $p > 0.05$) between 5-HT neurons projecting to different targets. The peptide CCK was not detected in any of the neurons tested.

Segregation of target-specific 5-HT neuronal populations using principal component analysis

A principal component analysis (PCA) was used on normalized electrophysiological data to determine the main axes of variation, and to derive common dimensional composites that can serve further classification purposes. Five principal components were extracted meeting Kaiser's criteria (Kaiser 1960), and were further considered in data rotation analysis. These components accounted for 83 % of the total variance observed in the dataset. Relative loadings of each current-clamp parameter to all extracted PCs are shown on Table 2. Regression scores for PC1, PC2 and PC3 are plotted in Fig. 4. Comparison of rotated PC1 vs PC2, and of PC1 vs PC3 values for each subpopulation of 5-HT neurons revealed a differential distribution of BLA-projection cells from mPFC- and dHP-projection neurons (Fig. 4). This result supports the notion that BLA-projecting neurons are intrinsically distinct and may constitute a subclass of 5-HT raphe neurons.

Unsupervised classification of 5-HT neurons in the raphe

To test the validity of these observations, and to identify and define serotonergic cell subclasses, we performed an unsupervised cluster analysis using Ward's method (Ward

Table 2 Rotated component matrix depicting the relative contribution of each current-clamp parameter

Parameter	PC1	PC2	PC3	PC4	PC5
Membrane potential (mV)	0.523	0.237	0.335	-0.259	-0.348
Input resistance ($M\Omega$)	-0.848	0.458	-0.237	-0.171	-0.281
Time constant (ms)	-0.770	0.115	-0.358	-0.287	-0.297
Capacitance (pF)	-0.030	-0.432	-0.241	-0.131	-0.012
Rheobase (pA)	0.378	-0.863	0.124	0.105	0.399
First spike latency (ms)	-0.206	-0.657	-0.541	-0.228	0.122
Action potential threshold (mV)	0.391	0.705	-0.458	0.005	-0.076
Action potential amplitude (mV)	-0.317	-0.776	0.313	-0.252	-0.131
Action potential duration (ms)	-0.068	0.721	0.517	0.348	0.438
AHP potential amplitude (mV)	-0.520	0.263	0.538	0.019	0.371
AHP potential time peak (mV)	-0.808	0.052	0.031	0.164	0.321
AHP 50 % recovery (ms)	-0.792	-0.010	-0.276	0.252	-0.150
Amplitude of first spike in train (mV)	-0.107	-0.797	0.386	-0.237	-0.340
Amplitude of second spike in train (mV)	-0.048	-0.898	0.169	-0.140	-0.331
Amplitude of last spike in train (mV)	0.145	-0.893	0.075	0.164	-0.223
Last train spike amplitude reduction	0.194	-0.310	-0.700	0.361	0.032
Maximal frequency (Hz)	0.337	-0.446	-0.333	0.535	0.033
Latency to first spike in a train (ms)	0.263	0.706	0.086	0.135	-0.588
Amplitude of early frequency adaptation (Hz)	-0.384	-0.814	-0.477	-0.184	0.381
Time constant of early adaptation (ms)	0.315	0.611	0.044	-0.142	0.105
maximal steady-state frequency (Hz)	-0.296	0.030	0.399	0.111	-0.103
Slope of late adaptation (Hz/ms)	0.528	0.402	-0.145	-0.625	-0.121

Parameters that heavily weighted individual components are marked in bold (cut-off = 0.7)

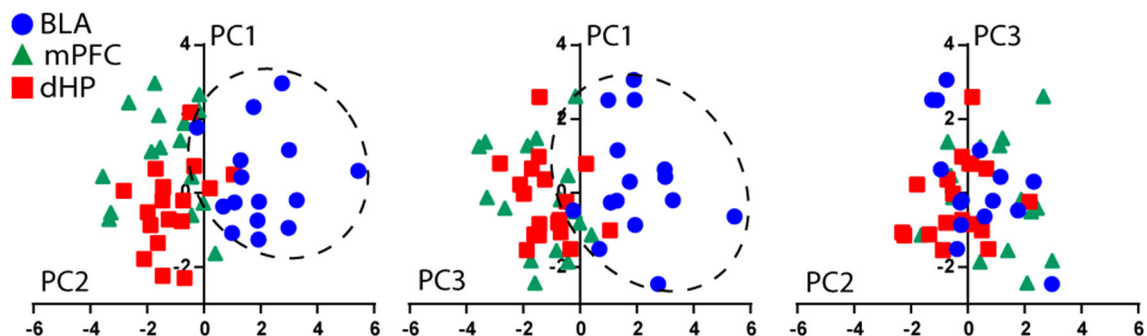
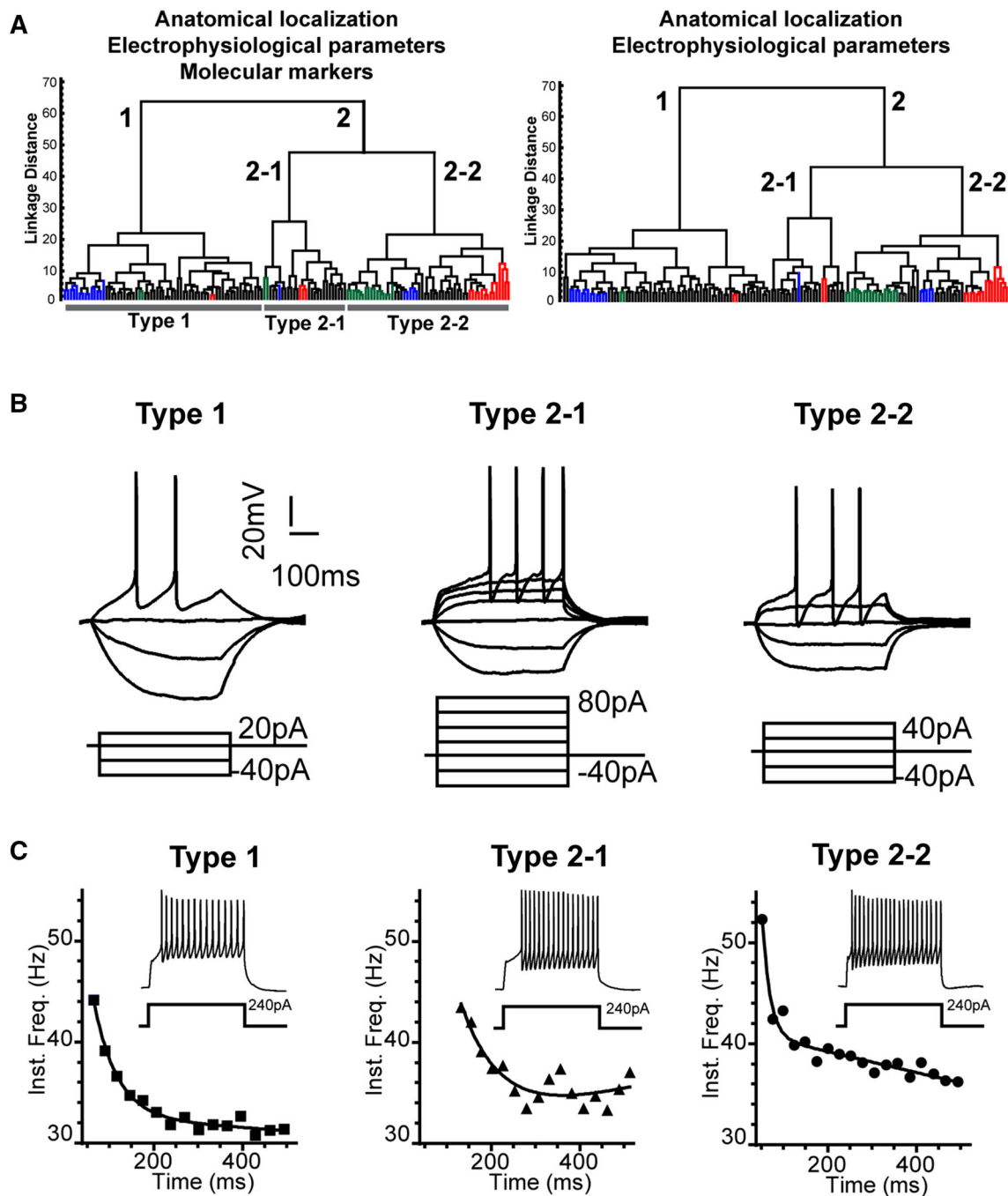


Fig. 4 Serotonergic cells projecting to the BLA segregate from mPFC and dHP projecting neurons in principal component space. Five principal components were extracted (83 % of total variance) and further considered in data rotation analysis. Relative loadings of each current-clamp parameter to all extracted PCs are shown on

Table 2. Comparison of rotated PC1 vs PC2, and of PC1 vs PC3 values for each subpopulation of 5-HT neurons revealed a differential distribution of BLA-projection cells from mPFC- and dHP-projection neurons

1963), a strategy that has been extensively used to classify neuronal classes based on multi-scale criteria (Cauli et al. 2000; Karagiannis et al. 2009). This method groups neurons with large similarities into high-order clusters where members share a number of common features. In each step, high-order clusters are grouped into new clusters of lower order until individual cases are completely segregated from one another. A clustering tree, called a dendrogram, is obtained to depict the arrangement of clusters with the

individual cells represented at the bottom (Fig. 5a). To obtain a representative sample suitable for a classification analysis, additional data were collected from 95 eGFP + serotonergic cells recorded in three areas of the raphe: the DR, in its medial (DRM) or lateral areas (DRL), and the MR. All serotonergic neurons were electrophysiologically characterized and subsequently analyzed by scRT-PCR as in the previous experiment; the neurons included in the study were all positive for the 5-HT



synthesizing enzyme Tph2. Classification was based on a total of 24 parameters, including anatomical localization, electrophysiological features and molecular phenotype. Figure 5a shows the results of a cluster analysis on the total sample of the 153 neurons analyzed (including 58 neurons with target identification and 95 with no target identification). Application of the Thorndike procedure resulted in three different cell types for the total population of 5-HT cells studied, corresponding to the branches 1 ($n = 67$), 2-1 ($n = 28$) and 2-2 ($n = 58$). To test the robustness of

this classification, we reduced the number of parameters and performed a cluster analysis based solely on electrophysiological parameters and anatomical localization. The resulting dendrogram, shown in Fig. 5a, retains a high degree of similarity in the main clusters and its members when compared with the dendrogram obtained when the molecular markers were also included.

Serotonergic neurons first segregated into two clusters. Neurons in the cluster 1 ($n = 67$) contained the majority of the BLA-projecting neurons (14/19), and are characterized

Fig. 5 Classification of 5-HT neurons by unsupervised cluster analysis. **a** Dendrogram showing the classification obtained based on anatomical, electrophysiological and molecular parameters from 153 cells. The *x* axis represents the individuals and the *y* axis the average within-cluster linkage distance. As determined by the Thorndike procedures (see “Materials and methods”), 5-HT neurons were segregated into three major clusters: type 1 ($n = 67$), type 2–1 ($n = 28$) and type 2–2 ($n = 58$). Serotonergic cells with distinct target projections were distributed in different cell groups. dHP (in *red*) and mPFC-projecting (in *green*) neurons are located mostly in the cluster 2–2, while neurons innervating the BLA (in *blue*) are mostly in group 1. A second dendrogram was obtained as a result of performing the same analysis but without including molecular criteria (*right*). Both analysis yielded similar results in the number of high-order clusters, the identity of cluster members and the segregation of cells with different target projections. **b** Representative voltage traces showing the response to increasing depolarizing current steps in the different cell types. Note that 5-HT neurons in branch 2–1 require higher current injections to discharge action potentials. For cluster group mean values and statistical comparisons for all electrophysiological parameters refer to Table 3. **c** Instantaneous frequency plots for the 5-HT neuronal types 1, 2–1 and 2–2. To account for the early and late frequency adaptation phenomena, instantaneous frequency was fitted to a single exponential with a sloping baseline. Representative voltage traces for each sub-type are shown. Cells in the cluster 2–1 showed low levels of spike frequency adaptation and were the only neuronal class that showed positive slope in the late adaptation phase, suggesting that these cells accelerate their firing rate after a first step of adaptation. Type 2–2 cells showed significantly higher discharge frequency and early adaptation

by significantly larger time constant and high input resistance (Fig. 5a; Table 3). As shown for BLA-field neurons (Figs. 2, 3), cluster 1 cells discharge slow action potentials of large amplitude, followed by a long-lasting AHP (Table 3). The second branch of the dendrogram is further subdivided into two second-order branches (Fig. 5a). Cluster 2–1 ($n = 28$) integrate only a few 5-HT cells with one of the 3 target projections analyzed. This group is characterized by the low excitability of its members, reflected by the high values of rheobase, action potential threshold and latency to first spike (Fig. 5b; Table 3). These cells showed low levels of spike frequency adaptation and were the only neuronal class that showed positive slope in the late adaptation phase, suggesting that these cells accelerate their firing rate after a first step of adaptation (Fig. 5c; Table 3). Cluster 2–2 contained the majority of dHP (14/19) and mPFC-projecting (16/20) 5-HT cells, although arranged in distinct lower order branches (Fig. 5a). Characterizing passive membrane properties in this group were low capacitance and fast time constant (Table 3), which would likely explain their ability to discharge at larger frequencies than the other two groups (Fig. 5b, c; Table 3). They also showed the highest levels of early frequency adaptation compared to group 1 and group 2–1, and a significantly higher maximum steady-state (Fig. 5c; Table 3).

Neurochemical identity of 5-HT cell clusters

The presence or absence of 20 genes across our sample of 153 5-HT cells is depicted as a heatmap in Fig. 6a, highlighting the different clusters. Genes such as CCK, CRF1 and NK1 were only rarely detected in the sample analyzed and are, thus, not useful discriminants. Molecular markers related with phenotypic characteristics seemed to yield the best discriminant power. For example, the number of cells expressing galanin was significantly higher in neurons of cluster 2–2 (68 %) compared to clusters 1 (10 %) and 2–1 (7 %) ($\epsilon = 3.56$, $p < 0.001$, Fig. 6b). Similarly, tachykinin 1 was more frequently found in the neurons of branch 2–2 (23 %), compared to type 1 (7 %) and type 2–1 (5 %) ($\epsilon = 3.56$, $p < 0.05$, Fig. 5c). Serotonergic neurons in the cluster 2–1 expressed Vg3 significantly more frequently (61 %) than clusters 1 (4 %) and 2–2 (5 %) ($\epsilon = 3.78$, $p < 0.001$, Fig. 6b). NOS expression, which has previously been reported to be differently expressed in the subcortical/cortical raphe projections (Simpson et al. 2003) was not discriminative for the present raphe neuronal subclasses, being expressed in about 50 % of cells of each cluster.

In contrast with the expression of co-transmission genes, expression of post-synaptic excitatory and inhibitory receptors showed no consistent variation between clusters (Fig. 5c). Adrenergic, orexinergic and histaminergic receptors were the most abundantly expressed in 5-HT neurons, but their presence was similar in all clusters. Similarly, molecular markers of inhibitory receptors, such as 5-HT1A, GABA_A, and GABA_B were evenly expressed across the three 5-HT subclasses (Fig. 6b). Overall, these results indicated that genes related with co-neurotransmission could be used as discriminative markers of electrophysiologically identified neurons projecting to different forebrain targets.

Topographical distribution of 5-HT cell clusters

Because previous observations (Beck et al. 2004a; Calizo et al. 2011) indicated differences in neuronal excitability between raphe sub-fields, it is of interest to determine whether topography can be a useful indicator of the serotonergic cell classes defined here. Supporting this notion, the DRL contained 90 % of group 1 cells and the MR contained 80 % of group 2–2 cells (Fig. 7, Table S1). In contrast, the DRM appeared to be the most heterogeneous subregion with 46 % type 1, 24 % type 2–1, and 30 % type 2–2 cells (Fig. 7, Table S1). Interestingly, target-specific subtypes were present within this subregion, since neurons projecting to the BLA were of type 1–1, whereas neurons projecting to the mPFC were of type 2–2. Thus, topography in itself is not sufficient to predict the 5-HT cell class, and

Table 3 Electrophysiological properties of 5-HT cell types

Parameter	Type 1 (<i>n</i> = 67)		Type 2–1 (<i>n</i> = 28)		Type 2–2 (<i>n</i> = 58)		Statistical comparison (Kruskal–Wallis, <i>p</i> values)		
	Mean	SEM	Mean	SEM	Mean	SEM	Type 1 vs 2–1	Type 1 vs 2–2	Type 2–1 vs 2–2
Membrane potential (mV)	−59.22	0.59	−62.46	1.40	−57.69	0.56	0.112718	0.052174	<i>0.005821</i>
Input resistance (MΩ)	1098.99	41.77	667.96	70.56	1061.18	67.11	<i>0.000001</i>	0.223552	<i>0.000153</i>
Time constant (ms)	100.38	5.05	59.54	7.83	69.05	4.66	<i>0.000009</i>	<i>0.000025</i>	0.137399
Capacitance (pF)	90.60	3.19	88.72	7.74	68.07	4.11	0.226897	<i>0.000000</i>	<i>0.006780</i>
Rheobase (pA)	18.51	1.61	72.14	8.25	28.73	3.15	<i>0.000000</i>	<i>0.006600</i>	<i>0.000000</i>
First spike latency (ms)	141.80	11.03	208.91	25.54	124.70	14.28	<i>0.012340</i>	0.056740	<i>0.000978</i>
Action potential threshold (mV)	−41.57	0.50	−37.13	0.80	−39.74	0.54	<i>0.000002</i>	<i>0.023841</i>	<i>0.010252</i>
Action potential amplitude (mV)	79.07	1.13	71.68	1.73	74.66	1.24	<i>0.000055</i>	<i>0.008753</i>	0.096802
Action potential duration (ms)	1.80	0.07	1.54	0.07	1.40	0.03	<i>0.025521</i>	<i>0.000019</i>	0.330379
AHP potential amplitude (mV)	−15.76	0.45	−18.88	0.78	−19.12	0.37	<i>0.001067</i>	<i>0.000000</i>	0.866980
AHP potential time peak (mV)	34.18	1.50	20.89	1.93	20.23	1.19	<i>0.000001</i>	<i>0.000000</i>	0.912358
AHP 50 % recovery (ms)	75.86	3.34	42.61	4.68	52.25	3.47	<i>0.000001</i>	<i>0.000001</i>	0.412535
Amplitude of first spike in train (mV)	71.04	1.12	68.00	1.65	69.22	1.10	0.069166	0.183320	0.412535
Amplitude of second spike in train (mV)	68.33	1.02	66.13	1.52	65.98	1.10	0.118433	0.075815	0.942777
Amplitude of last spike in train (mV)	63.41	1.01	62.24	1.67	59.76	1.49	0.360562	0.066864	0.517902
Last train spike amplitude reduction	0.90	0.01	0.92	0.01	0.87	0.02	0.112718	0.429508	0.102817
Maximal frequency (Hz)	31.34	0.74	29.71	1.73	40.98	1.40	0.600554	<i>0.000000</i>	<i>0.000005</i>
Latency to first spike in a train (ms)	28.77	1.68	50.70	6.40	19.98	2.35	<i>0.000734</i>	<i>0.001257</i>	<i>0.000016</i>
Amplitude of early frequency adaptation (Hz)	11.60	0.59	7.70	1.79	15.87	1.82	0.126400	<i>0.009598</i>	<i>0.002279</i>
Time constant of early adaptation (ms)	46.95	2.53	32.27	6.20	32.92	3.03	<i>0.005126</i>	<i>0.000004</i>	0.562299
maximal steady-state frequency (Hz)	32.12	0.73	31.84	2.10	43.03	1.36	0.711933	<i>0.000000</i>	<i>0.000038</i>
Slope of late adaptation (Hz/ms)	−0.0065	0.0007	0.0023	0.0024	−0.0086	0.0013	<i>0.000020</i>	0.278723	<i>0.000009</i>

Electrophysiological parameters were measured as described in “Materials and methods”. *p* values in italics denote statistical significance

heterogeneity within the DRM needs to be taken into account.

Discussion

Accumulating evidence suggests that 5-HT heterogeneity is key to understand how this small group of cells participates in many different biological functions (Calizo et al. 2011; Hale and Lowry 2011; Gaspar and Lillesaar 2012). Previous efforts to characterize 5-HT neurons have relied on independent morphological (Molliver 1987), molecular (Larm et al. 2003; Aznar et al. 2005; Lacoste et al. 2006; Amilhon et al. 2010; Fu et al. 2010; Spaethling et al. 2014) or electrophysiological features (Kirby et al. 2003; Hajós et al. 2007; Calizo et al. 2011). Here, we carried out a

characterization and classification of 5-HT neurons based on a multi-scale analysis. We focused on the serotonergic innervation of limbic structures, i.e., the amygdala, the hippocampus and the mPFC, that are main components of anatomically and functionally related circuits involved in adaptive and pathological emotional behaviors (LeDoux 2000). We observed that 5-HT neurons that project to the dHP, the mPFC, and the BLA constitute essentially separate subpopulations of neurons, although they partly overlap topographically in the DRM and MR. The fact that a majority of 5-HT raphe neurons send separate axonal projections to the mPFC, dHP and BLA, does not mean that individual neurons innervate a single target region. Rather, it means that within the constraints of our experiments we did not observe a significant number of neurons with dual projections; indeed anterograde tracing

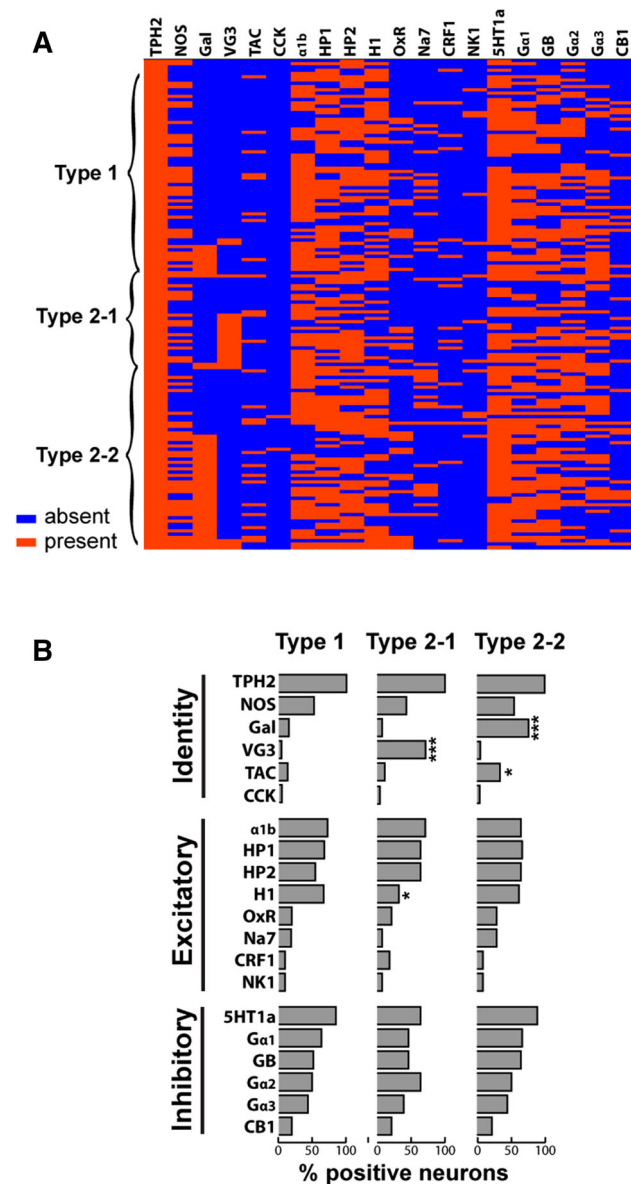
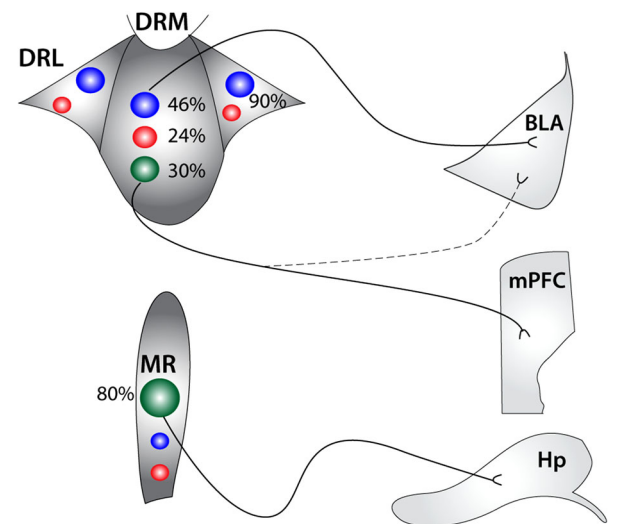


Fig. 6 Molecular identity of 5-HT cell clusters. **a** Heatmap of genes expression across the different 5-HT cell clusters obtained by single-cell RT-PCR (total sample of 153 5-HT neurons). Genes were either present (orange) or absent (blue) in a particular cell if a DNA band of the predicted size was revealed by electrophoresis in agarose after two rounds of amplification. **b** Bar graphs represent the % of cells within the group that were positive for a particular gene. All cells expressed the 5-HT synthesizing enzyme Tph2. The % of cells expressing galanin was significantly higher in neurons of cluster 2–2 (68 %) compared to clusters 1 (10 %) and 2–1 (7 %) ($\epsilon = 3.56, p < 0.001$). Tachykinin 1 was more frequently found in the neurons of branch 2–2 (23 %), compared to type 1 (7 %) and type 2–1 (5 %) ($\epsilon = 3.56, p < 0.05$). Serotonergic neurons in the cluster 2–1 expressed Vg3 significantly more frequently (61 %) than clusters 1 (4 %) and 2-2 (5 %) ($\epsilon = 3.78, p < 0.001$). *Tph2* tryptophan hydroxylase 2, *NOS* nitric oxide synthase, *Gal* galanin, *Vg3* vesicular glutamate transporter 3, *TAC* tachykinin, *CCK* cholecystokinin, α 1b adrenergic α 1b receptor subunit, *HP1* and *HP2* hypocretin receptors, *H1* histamine 1 receptor, *OxR* oxytocin receptor, *Na7* nicotinic α 7 receptor, *CRF1* corticotrophin-releasing factor receptor 1, *NK1* neurokinin 1 receptor, *Ga1, 2* and *3* GABAA receptor α subunits, *GB* GABAB receptor 1a subunit, *CB1* cannabinoid receptor

experiments of single raphe neurons has shown the complexity of individual axonal arbors arising from the raphe (Gagnon and Parent 2014). A major finding of the present study was that 5-HT neurons projecting to the dHP and the mPFC were different from BLA-projecting neurons in excitability, membrane properties and by the expression of the peptide galanin. Further unsupervised cluster analysis of 5-HT raphe neurons, allowed to define three functional subsets of serotonergic cells based on the combination of anatomical, electrophysiological and molecular features. The existence of 5-HT neuronal classes and their specificity in forebrain target innervation have significant implications in the way serotonergic signalling is conceived.

The results presented here could add significantly to our understanding of how 5-HT patterns of release are



Class	Excitability	AP	AHP	Marker
Type 1	↓	wide	slow	?
Type 2-1	↓↓	narrow	fast	Vg3
Type 2-2	↑	narrow	fast	galanin

Fig. 7 Summary of 5-HT neuronal types' topographic distribution in the raphe and innervation targets. The dorsal raphe medialis (DRM) is the most heterogeneous area showing similar abundance of the three characterized cell types. The median raphe (MR) contains 80 % of type 2–2 cells, and the dorsal raphe lateral (DRL) 90 % of type 1 neurons. Type 2–2 5-HT cells located in the MR and DR send axonal projections to the dorsal hippocampus (dHP) and the medial prefrontal cortex (mPFC), respectively. The basolateral amygdala (BLA) is mostly innervated by type 1 neurons located in the DR. The number of cells per group in each of the regions of the raphe is as follows: group 1, 26 cells in DR, 39 cells in DRL, 2 cells in MR; group 2–1, 14 cells in DR, 5 cells in DRL, 9 cells in MR; group 2–2, 17 cells in DR, 0 cells in DRL, 41 cells in MR

organized in the brain. Recent studies demonstrated that both DR and MR 5-HT raphe neurons receive direct monosynaptic inputs from a variety of glutamatergic, GABAergic and peptidergic neurons (Ogawa et al. 2014; Pollak Dorocic et al. 2014; Weissbourd et al. 2014) with some differences in the inputs to the DR and MR (Pollak Dorocic et al. 2014). However, our scRT-PCR analysis showed little variations in the expression of glutamatergic, GABAergic or peptide membrane receptors among the sample of 153 5-HT raphe neurons analyzed. Thus, differences in excitatory/inhibitory receptor expression do not contribute to the differences in excitability that were observed within the present sample. Rather, it is possible that variations in membrane properties ultimately define the way in which these neurons integrate multiple synaptic afferents from different sources (Soiza-Reilly and Commons 2014). For example, type 1 neurons have high membrane resistance and large time constant, properties that would permit to strongly enhance even small synaptic inputs and to increase the chances of temporal summation of individual events. We hypothesize that the raphe-amygdala pathway involving type 1 neurons form a sub-system that facilitates the rapid and transient release of 5-HT in the amygdala, for example in alert or startle responses. This is in accordance with recent studies showing that this pathway is under inhibitory control by reciprocal amygdala monosynaptic inputs to GABAergic neurons in the DR (Pollak Dorocic et al. 2014; Weissbourd et al. 2014).

Though most 5-HT neurons are regular, slow-spiking, some neurons in the DR can also discharge high frequency bursts of action potentials (Kocsis et al. 2006; Hajós et al. 2007). Tonic pacemaker activity in serotonergic neurons serves primarily to maintain 5-HT levels throughout the brain, while phasic bursts are stimulus-specific responses delivering fine temporal and spatial synaptic information (McQuade and Sharp 1995; Gartside et al. 2000; Hajós et al. 2007; Ranade and Mainen 2009; Schweimer and Ungless 2010; Miyazaki et al. 2011). In this study, our results show that 5-HT neurons *in vitro* also present differences in discharge frequency. Serotonergic neurons in the cluster 2–2 were characterized by having a small time constant, which allows them to rapidly charge their membrane, and by discharging short spikes followed by a fast AHP. Although, present experiments cannot confirm that these cells would assume bursting activity *in vivo*, their intrinsic properties would suggest so. Induction of bursting firing, and hence potentiation of 5-HT transmission could be a new therapeutic avenue in neuropsychiatry (Blank et al. 2004). Our results pinpoint group 2–2 cells as an interesting candidate to further our understanding of bursting firing behavior. However, further studies will be needed to

correlate our findings with *in vivo* discharge behaviors shown by 5-HT neurons.

Previous studies have shown that a subpopulation of 5-HT neurons express the vesicular glutamate transporter Vg3 (Gras et al. 2002; Schäfer et al. 2002), and we showed here that these neurons segregated into a subclass, type 2–1, easily identifiable by their low excitability and long firing delay. The expression of Vg3 in 5-HT neurons has been linked to the co-release of glutamate that evokes fast excitatory co-transmission at postsynaptic targets (Johnson 1994; Varga et al. 2009; Liu et al. 2014). In addition, Vg3 enhances vesicular filling, and Vg3 + serotonergic fibers have enhanced release because they pack more 5-HT in their vesicles (Gras et al. 2008; Amilhon et al. 2010). Both lines of evidence suggest that this neuronal subpopulation constitutes a specialized type of serotonergic signaling, featuring fast and boosted transmission. Interestingly, our results showed that these neurons have a high discharge threshold, suggesting that Vg3 + serotonergic neurons could be independently recruited at higher regimes of excitatory afferents. Overall, it seems that this sub-system is designed as a reservoir conveying boosted serotonergic/glutamatergic signals. The functional significance of this subpopulation of 5-HT neurons was recently asserted in an elegant study showing that both 5-HT and glutamate contribute to the reward signal encoded in the DR cells (Liu et al. 2014). This suggests that Vg3 + 5-HT neurons may preferentially project to reward-related structures, such as the VTA and the nucleus accumbens, explaining why we did not find great number of type 2–1 neurons projecting to the BLA, the mPFC or the dHP.

One unexpected finding from this study was the topographic distribution of 5-HT neuronal types across raphe subdivisions. The DRM appeared to be the most heterogeneous area, with equal abundance of all three cell types. This raphe sub-division contains the 5-HT cells that send axonal projections to the BLA and the mPFC, mainly through discrete pathways. Because recordings were essentially done in the rostral part of the DRM, it is unlikely that the rostral to caudal heterogeneity of the DR (Muzerelle et al. 2014; Commons 2015) contributes to these differences. Conversely, the DRL and MR were more homogeneous, being essentially composed of one subtype (type 1 in the DRL and type 2–2 in the MR). For example, Beck et al. showed that 5-HT neurons in the MR have shorter time constant than DR neurons, consistent with our proposed model that the MR is composed mostly of type 2–2 cells (Table 3) (Beck et al. 2004b). These results, suggest that anatomically defined raphe subfields can comprise diverse 5-HT neuronal types rather than a homogenous population of cells. Thus, electrophysiological and neurochemical tags that would allow the identification and targeting of these cell types are most desirable.

The present study correlates the expression of the peptide galanin with a subpopulation of fast-spiking 5-HT neurons located in the DRM and targeting the mPFC and the dHP. In addition, we reveal the existence of an atypical subtype of 5-HT that expresses Vg3 that combined low excitability and long discharge delays.

Distinct neuronal cell types acquire and maintain their identity by expressing different genes, and recent studies have yielded remarkable insights into serotonergic genetic differentiation. For example, whole-genome expression profiling studies have demonstrated a duality in the anterior and posterior 5-HT cells groups (Wylie et al. 2010). Serotonergic neurons in the anterior group, including the DR and MR, derive from rhombomeres 1–3 (Jensen et al. 2008; Bang et al. 2012; Alonso et al. 2012). Using intersectional genetic cell-fating, Jensen et al. demonstrated that DR neurons derive exclusively from rhombomere 1 while the MR neurons arise from progenitors in rhombomeres 1, 2 and 3 (Jensen et al. 2008). From this evidence, one would expect a greater degree of diversity within the MR than the DR; contrasting with the results here that showed the existence of three 5-HT cell types in the DR. Nevertheless, transcriptional cascades that are required for serotonergic neuronal specification are highly complex, and it is possible that later stages of maturation are fundamental in the programming of 5-HT cell types (Hendricks et al. 2003). For instance, after genetic deletion of the transcription factor *Pet1* a significant loss in the number of 5-HT cells in the raphe has been noted; however, a 20–30 % subpopulation in both the DR and the MR remains (Hendricks et al. 2003; Kiyasova et al. 2011). The distribution of the remaining 5-HT cells revealed that *Pet1*-resistant 5-HT neurons have highly organized target innervation patterns. For example, serotonergic fibers to the mPFC and the hippocampus are absent, while projections to the BLA remain intact (Kiyasova et al. 2011), suggesting a crucial heterogeneity in the differentiation pathways involving neurons innervating different forebrain targets. We show that 5-HT neurons projecting to the BLA have a distinct phenotype and segregate from those projecting to the mPFC and dorsal hippocampus suggesting that *Pet1*-resistant neurons would have phenotypic characteristics similar to the BLA-projecting type 1 neurons. Further studies are necessary to corroborate this hypothesis and further our understanding of how a mosaic of neurons with different connective and functional identities may be constructed during development.

Acknowledgments This work was funded by INSERM, the University Pierre et Marie Curie, the European Commission (FP7-health-2007-A-201714), The Fondation pour la Recherche Medicale (equipe FRM to PG) and the Agence Nationale pour la recherche (ANR605-neur-046 and ANR 2011 MALZ 003 01). SPF received a Fellowship from the Fondation pour la Recherche Medicale. The teams of PG and JCP are part of the Ecole de Neurosciences de Paris

(ENP) training network and Labex Bio-Psy (Investissement d'Avenir, ANR). We thank Evan Deneris and Gord Fishell for providing the founders of *ePet1-Cre* and *RCE:LoxP* mouse lines. Sophie Scottotomassese is acknowledged for help with confocal microscopy and Emma Martinelli and Mariano Soiza-Reilly for their helpful comments on the manuscript. The authors declare no competing financial interests.

References

- Aghajanian GK, Vandermaelen CP (1982) Intracellular recordings from serotonergic dorsal raphe neurons: pacemaker potentials and the effect of LSD. *Brain Res* 238:463–469
- Alonso A, Merchán P, Sandoval JE, Sánchez-Arrones L, Garcia-Cazorla A, Artuch R, Ferrán JL, Martínez-de-la-Torre M, Puelles L (2012) Development of the serotonergic cells in murine raphe nuclei and their relations with rhombomeric domains. *Brain Struct Funct* 18:1229–1277
- Amilhon B, Lepicard E, Renoir T, Mongeau R, Popa D, Poirel O, Miot S, Gras C, Gardier AM, Gallego J, Hamon M, Lanfumey L, Gasnier B, Giros B, El Mestikawy S (2010) VGLUT3 (vesicular glutamate transporter type 3) contribution to the regulation of serotonergic transmission and anxiety. *J Neurosci* 30:2198–2210
- Andrade R, Haj-Dahmane S (2013) Serotonin neuron diversity in the dorsal raphe. *ACS Chem Neurosci* 4:22–25
- Aznar S, Kostova V, Christiansen SH, Knudsen GM (2005) Alpha 7 nicotinic receptor subunit is present on serotonin neurons projecting to hippocampus and septum. *Synapse* 55:196–200
- Bang SJ, Jensen P, Dymecki SM, Commons KG (2012) Projections and interconnections of genetically defined serotonin neurons in mice. *Eur J Neurosci* 35:85–96
- Beck SG, Pan Y-Z, Akanwa AC, Kirby LG (2004a) Median and dorsal raphe neurons are not electrophysiologically identical. *J Neurophysiol* 91:994–1005
- Beck SG, Pan Y-Z, Akanwa AC, Kirby LG (2004b) Median and dorsal raphe neurons are not electrophysiologically identical. *J Neurophysiol* 91:994–1005
- Blank T, Nijholt I, Kye M-J, Spiess J (2004) Small conductance Ca^{2+} -activated K^{+} channels as targets of CNS drug development. *Curr Drug Targets CNS Neurol Disord* 3:161–167
- Brust RD, Corcoran AE, Richerson GB, Nattie E, Dymecki SM (2014) Functional and developmental identification of a molecular subtype of brain serotonergic neuron specialized to regulate breathing dynamics. *Cell Rep* 9:2152–2165
- Buhot MC, Martin S, Segu L (2000) Role of serotonin in memory impairment. *Ann Med* 32:210–221
- Bunin MA, Wightman RM (1999) Paracrine neurotransmission in the CNS: involvement of 5-HT. *Trends Neurosci* 22:377–382
- Calizo LH, Akanwa A, Ma X, Pan Y-Z, Lemos JC, Craig C, Heemstra LA, Beck SG (2011) Raphe serotonin neurons are not homogenous: electrophysiological, morphological and neurochemical evidence. *Neuropharmacology* 61:524–543
- Cauli B, Porter JT, Tsuzuki K, Lambiez B, Rossier J, Quenet B, Audinat E (2000) Classification of fusiform neocortical interneurons based on unsupervised clustering. *Proc Natl Acad Sci USA* 97:6144–6149
- Chandler DJ, Gao W-J, Waterhouse BD (2014) Heterogeneous organization of the locus coeruleus projections to prefrontal and motor cortices. *Proc Natl Acad Sci USA* 111:6816–6821
- Chan-Palay V, Jonsson G, Palay SL (1978) Serotonin and substance P coexist in neurons of the rat's central nervous system. *Proc Natl Acad Sci USA* 75:1582–1586
- Commons KG (2015) Two major network domains in the dorsal raphe nucleus. *J Comp Neurol* 523:1488–1504

- Commons KG, Connolley KR, Valentino RJ (2003) A neurochemically distinct dorsal raphe-limbic circuit with a potential role in affective disorders. *Neuropsychopharmacology* 28:206–215
- Crawford LK, Craige CP, Beck SG (2010) Increased intrinsic excitability of lateral wing serotonin neurons of the dorsal raphe: a mechanism for selective activation in stress circuits. *J Neurophysiol* 103:2652–2663
- Deneris ES, Wyler SC (2012) Serotonergic transcriptional networks and potential importance to mental health. *Nat Neurosci* 15:519–527
- Fernandez SP, Gaspar P (2012) Investigating anxiety and depressive-like phenotypes in genetic mouse models of serotonin depletion. *Neuropharmacology* 62:144–154
- Fu W, Le Maître E, Fabre V, Bernard J-F, David Xu Z-Q, Hökfelt T (2010) Chemical neuroanatomy of the dorsal raphe nucleus and adjacent structures of the mouse brain. *J Comp Neurol* 518:3464–3494
- Gagnon D, Parent M (2014) Distribution of VGLUT3 in highly collateralized axons from the rat dorsal raphe nucleus as revealed by single-neuron reconstructions. *PLoS ONE* 9:e87709
- Gartside SE, Hajós-Korcsok E, Bagdy E, Hársing LG Jr, Sharp T, Hajós M (2000) Neurochemical and electrophysiological studies on the functional significance of burst firing in serotonergic neurons. *Neuroscience* 98:295–300
- Gaspar P, Lillesaar C (2012) Probing the diversity of serotonin neurons. *Philos Trans R Soc Lond B Biol Sci* 367:2382–2394
- Graeff FG, Zangrossi H Jr (2010) The dual role of serotonin in defense and the mode of action of antidepressants on generalized anxiety and panic disorders. *Cent Nerv Syst Agents Med Chem* 10:207–217
- Gras C, Herzog E, Belenchi GC, Bernard V, Ravassard P, Pohl M, Gasnier B, Giros B, El Mestikawy S (2002) A third vesicular glutamate transporter expressed by cholinergic and serotonergic neurons. *J Neurosci* 22:5442–5451
- Gras C, Amilhon B, Lepicard EM, Poirel O, Vinatier J, Herbin M, Dumas S, Tzavara ET, Wade MR, Nomikos GG, Hanoun N, Saurini F, Kemel M-L, Gasnier B, Giros B, El Mestikawy S (2008) The vesicular glutamate transporter VGLUT3 synergizes striatal acetylcholine tone. *Nat Neurosci* 11:292–300
- Hajós M, Allers KA, Jennings K, Sharp T, Charette G, Sfik A, Kocsis B (2007) Neurochemical identification of stereotypic burst-firing neurons in the rat dorsal raphe nucleus using juxtacellular labelling methods. *Eur J Neurosci* 25:119–126
- Hale MW, Lowry CA (2011) Functional topography of midbrain and pontine serotonergic systems: implications for synaptic regulation of serotonergic circuits. *Psychopharmacology* 213:243–264
- Hendricks TJ, Fyodorov DV, Wegman LJ, Lelutiu NB, Pehek EA, Yamamoto B, Silver J, Weeber EJ, Sweatt JD, Deneris ES (2003) Pet-1 ETS gene plays a critical role in 5-HT neuron development and is required for normal anxiety-like and aggressive behavior. *Neuron* 37:233–247
- Hensler JG (2006) Serotonergic modulation of the limbic system. *Neurosci Biobehav Rev* 30:203–214
- Hill EL, Gallopin T, Férézou I, Cauli B, Rossier J, Schweitzer P, Lambollez B (2007) Functional CB1 receptors are broadly expressed in neocortical GABAergic and glutamatergic neurons. *J Neurophysiol* 97:2580–2589
- Jacobs BL, Foote SL, Bloom FE (1978) Differential projections of neurons within the dorsal raphe nucleus of the rat: a horseradish peroxidase (HRP) study. *Brain Res* 147:149–153
- Jensen P, Farago AF, Awatramani RB, Scott MM, Deneris ES, Dymecki SM (2008) Redefining the serotonergic system by genetic lineage. *Nat Neurosci* 11:417–419
- Johnson MD (1994) Synaptic glutamate release by postnatal rat serotonergic neurons in microculture. *Neuron* 12:433–442
- Johnson MD, Yee AG (1995) Ultrastructure of electrophysiologically-characterized synapses formed by serotonergic raphe neurons in culture. *Neuroscience* 67:609–623
- Kaiser HF (1960) The application of electronic computers to factor analysis. *Educ Psychol Measur* 20:141–151
- Karagiannis A, Gallopin T, Dávid C, Battaglia D, Geoffroy H, Rossier J, Hillman EMC, Staiger JF, Cauli B (2009) Classification of NPY-expressing neocortical interneurons. *J Neurosci* 29:3642–3659
- Kirby LG, Pernar L, Valentino RJ, Beck SG (2003) Distinguishing characteristics of serotonin and non-serotonin-containing cells in the dorsal raphe nucleus: electrophysiological and immunohistochemical studies. *Neuroscience* 116:669–683
- Kiyasova V, Fernandez SP, Laine J, Stankovski L, Muzerelle A, Doly S, Gaspar P (2011) A genetically defined morphologically and functionally unique subset of 5-HT neurons in the mouse raphe nuclei. *J Neurosci* 31:2756–2768
- Kiyasova V, Bonnavion P, Scotto-Lomassese S, Fabre V, Sahly I, Tronche F, Deneris E, Gaspar P, Fernandez SP (2013) A subpopulation of serotonergic neurons that do not express the 5-HT1A autoreceptor. *ACS Chem Neurosci* 4:89–95
- Kocsis B, Varga V, Dahan L, Sik A (2006) Serotonergic neuron diversity: identification of raphe neurons with discharges time-locked to the hippocampal theta rhythm. *Proc Natl Acad Sci USA* 103:1059–1064
- Köhler C, Steinbusch H (1982) Identification of serotonin and non-serotonin-containing neurons of the mid-brain raphe projecting to the entorhinal area and the hippocampal formation. A combined immunohistochemical and fluorescent retrograde tracing study in the rat brain. *Neuroscience* 7:951–975
- Lacoste B, Riad M, Descarries L (2006) Immunocytochemical evidence for the existence of substance P receptor (NK1) in serotonin neurons of rat and mouse dorsal raphe nucleus. *Eur J Neurosci* 23:2947–2958
- Lammel S, Hetzel A, Häckel O, Jones I, Liss B, Roeper J (2008) Unique properties of mesoprefrontal neurons within a dual mesocorticolimbic dopamine system. *Neuron* 57:760–773
- Larm JA, Shen P-J, Gundlach AL (2003) Differential galanin receptor-1 and galanin expression by 5-HT neurons in dorsal raphe nucleus of rat and mouse: evidence for species-dependent modulation of serotonin transmission. *Eur J Neurosci* 17:481–493
- LeDoux JE (2000) Emotion circuits in the brain. *Annu Rev Neurosci* 23:155–184
- Liu Z, Zhou J, Li Y, Hu F, Lu Y, Ma M, Feng Q, Zhang J-E, Wang D, Zeng J, Bao J, Kim J-Y, Chen Z-F, El Mestikawy S, Luo M (2014) Dorsal raphe neurons signal reward through 5-HT and glutamate. *Neuron* 81:1360–1374
- Margolis EB, Mitchell JM, Ishikawa J, Hjelmstad GO, Fields HL (2008) Midbrain dopamine neurons: projection target determines action potential duration and dopamine D(2) receptor inhibition. *J Neurosci* 28:8908–8913
- McQuade R, Sharp T (1995) Release of cerebral 5-hydroxytryptamine evoked by electrical stimulation of the dorsal and median raphe nuclei: effect of a neurotoxic amphetamine. *Neuroscience* 68:1079–1088
- Melander T, Hökfelt T, Rökaeus A, Cuello AC, Oertel WH, Verhofstad A, Goldstein M (1986) Coexistence of galanin-like immunoreactivity with catecholamines, 5-hydroxytryptamine, GABA and neuropeptides in the rat CNS. *J Neurosci* 6:3640–3654
- Miyazaki K, Miyazaki KW, Doya K (2011) Activation of dorsal raphe serotonin neurons underlies waiting for delayed rewards. *J Neurosci* 31:469–479
- Miyazaki K, Miyazaki KW, Doya K (2012) The role of serotonin in the regulation of patience and impulsivity. *Mol Neurobiol* 45:213–224

- Molliver ME (1987) Serotonergic neuronal systems: what their anatomic organization tells us about function. *J Clin Psychopharmacol* 7:3S–23S
- Muzerelle A, Scotto-Lomassese S, Bernard JF, Soiza-Reilly M, Gaspar P (2014) Conditional anterograde tracing reveals distinct targeting of individual serotonin cell groups (B5-B9) to the forebrain and brainstem. *Brain Struct Funct* 1–27. doi:10.1007/s00429-014-0924-4
- Ogawa SK, Cohen JY, Hwang D, Uchida N, Watabe-Uchida M (2014) Organization of monosynaptic inputs to the serotonin and dopamine neuromodulatory systems. *Cell Rep* 8:1105–1118
- Pollak Dorocic I, Fürth D, Xuan Y, Johansson Y, Pozzi L, Silberberg G, Carlén M, Meletis K (2014) A whole-brain atlas of inputs to serotonergic neurons of the dorsal and median raphe nuclei. *Neuron* 83:663–678
- Ranade SP, Mainen ZF (2009) Transient firing of dorsal raphe neurons encodes diverse and specific sensory, motor, and reward events. *J Neurophysiol* 102:3026–3037
- Schäfer MK-H, Varoqui H, Defamie N, Weihe E, Erickson JD (2002) Molecular cloning and functional identification of mouse vesicular glutamate transporter 3 and its expression in subsets of novel excitatory neurons. *J Biol Chem* 277:50734–50748
- Schweimer JV, Ungless MA (2010) Phasic responses in dorsal raphe serotonin neurons to noxious stimuli. *Neuroscience* 171:1209–1215
- Scott MM, Wylie CJ, Lerch JK, Murphy R, Lobur K, Herlitze S, Jiang W, Conlon RA, Strowbridge BW, Deneris ES (2005) A genetic approach to access serotonin neurons for in vivo and in vitro studies. *Proc Natl Acad Sci USA* 102:16472–16477
- Simpson KL, Waterhouse BD, Lin RCS (2003) Differential expression of nitric oxide in serotonergic projection neurons: neurochemical identification of dorsal raphe inputs to rodent trigeminal somatosensory targets. *J Comp Neurol* 466:495–512
- Soiza-Reilly M, Commons KG (2014) Unraveling the architecture of the dorsal raphe synaptic neuropil using high-resolution neuroanatomy. *Front Neural Circuits* 8:105
- Sousa VH, Miyoshi G, Hjerling-Leffler J, Karayannis T, Fishell G (2009) Characterization of Nk6–2-derived neocortical interneuron lineages. *Cereb Cortex* 19(Suppl 1):i1–i10
- Spaethling JM, Piel D, Dueck H, Buckley PT, Morris JF, Fisher SA, Lee J, Sul J-Y, Kim J, Bartfai T, Beck SG, Eberwine JH (2014) Serotonergic neuron regulation informed by in vivo single-cell transcriptomics. *FASEB J* 28:771–780
- Thorndike RL (1953) Who belongs in the family. *Psychometrika* 18:267–276
- Toutenburg H (1971) Fisher, R. A., and F. Yates: Statistical tables for biological, agricultural and medical research. 6th Ed. Oliver & Boyd, Edinburgh and London 1963. X, 146 P. Preis 42 s net. *Biometrische Zeitschrift* 13:285
- Trulsson ME, Frederickson CJ (1987) A comparison of the electrophysiological and pharmacological properties of serotonin-containing neurons in the nucleus raphe dorsalis, raphe medianus and raphe pallidus recorded from mouse brain slices in vitro: role of autoreceptors. *Brain Res Bull* 18:179–190
- Vandermaelen CP, Aghajanian GK (1983) Electrophysiological and pharmacological characterization of serotonergic dorsal raphe neurons recorded extracellularly and intracellularly in rat brain slices. *Brain Res* 289:109–119
- Varga V, Losonczy A, Zemelman BV, Borhegyi Z, Nyiri G, Domonkos A, Hangya B, Holderith N, Magee JC, Freund TF (2009) Fast synaptic subcortical control of hippocampal circuits. *Science* 326:449–453
- Vertes RP, Crane AM (1997) Distribution, quantification, and morphological characteristics of serotonin-immunoreactive cells of the suprallemniscal nucleus (B9) and pontomesencephalic reticular formation in the rat. *J Comp Neurol* 378:411–424
- Vertes RP, Fortin WJ, Crane AM (1999) Projections of the median raphe nucleus in the rat. *J Comp Neurol* 407:555–582
- Ward JH (1963) Hierarchical grouping to optimize an objective function. *J Am Stat Assoc* 58:236–244
- Waselus M, Valentino RJ, Van Bockstaele EJ (2011) Collateralized dorsal raphe nucleus projections: a mechanism for the integration of diverse functions during stress. *J Chem Neuroanat* 41:266–280
- Weissbourd B, Ren J, DeLoach KE, Guenther CJ, Miyamichi K, Luo L (2014) Presynaptic partners of dorsal raphe serotonergic and GABAergic neurons. *Neuron* 83:645–662
- Wylie CJ, Hendricks TJ, Zhang B, Wang L, Lu P, Leahy P, Fox S, Maeno H, Deneris ES (2010) Distinct transcriptomes define rostral and caudal serotonin neurons. *J Neurosci* 30:670–684